Upstream Non-Oscillatory Advection Schemes Suitable for Ocean Wave Models

Jian-Guo Li
Met Office, FitzRoy Road, Exeter, EX1 3PB, UK
Email: Jian-Guo.Li@metoffice.gov.uk

Abstract: The first order upstream advection scheme used in the WAM ocean wave models is known too diffusive and is responsible for the underestimation of long distance swells. High order advection schemes used in other wave models, like the 3rd order ULTIMATE QUICKEST scheme in WAVEWATCH III, are 'too good' as it does not smooth out the garden sprinkler effect. The purpose of this paper is to find a suitable 2nd order scheme, which reduces the 1st order diffusion but keeps enough smoothing for the discrete direction and spectral bins. Of course, it should be free from oscillations which haunt many high order schemes. The proposed upstream non-oscillatory 2nd order (UNO2) scheme is adapted from the MINMOD scheme and simplified to favour vectorization on super computers. The scheme is extended to 2-D with the multi-dimensional advective-conservative hybrid operator (MACHO), which keeps the 2-D scheme stable under the 1-D CFL condition and eliminates time-splitting errors. The scheme has been tested in the Met Office global and regional wave models. It is more effective than the 3rd order Gadd scheme used in the Met Office operational wave models and even shows better results than the old scheme. A 3rd order scheme (UNO3), similar to the 3rd order ULTIMATE QUICKEST scheme but replaced its flux limiter part by the UNO2 scheme, is also presented. The UNO3 scheme is of the same accuracy as the ULTIMATE QUICKEST scheme but more efficient. Two more intermediate schemes ($UNO2^+$ and $UNO3^-$) are derived from the van Leer homonic average. Classical numerical (1-D constant speed and 2-D solid rotation and deformation) tests have demonstrated that these schemes are non-oscillatory, conservative and shape-preserving. These schemes, especially the UNO2 scheme, are recommended for replacing the 1st order upstream scheme in WAM models.

1. Introduction

Advection is a fundamental physical process associated with many fluid applications, such as mass, energy, and tracer transportation in atmospheric and oceanic flows. The conservation of a fluid mass ψ with velocity $\mathbf{v}$ is represented by the advection equation:

$$\partial\psi/\partial t + \nabla \bullet (\mathbf{v}\psi) = 0 \tag{1}$$

where t represents the time and the space gradient operator is over all space dimensions. Translation of the advection equation into an accurate discrete form proved not to be straightforward though modellers have been searching for the 'perfect' one for many decades. The most frustrating obstacle in the development of advection schemes is numerical oscillation associated with high order schemes derived from apparently the most straightforward finite difference techniques.

Following the publication of the 1st order upstream scheme (Godunov 1959), many attempts to derive higher order schemes were plagued with numerical oscillations, including Lax and Wendroff (1960), Crowley (1968), Fromm (1968), Leonard (1979), Smolarkiewicz (1982), Takacs (1985) and Tremback et al (1987), to name just a few. A great deal of effort has been spent on suppressing these spurious oscillations and led to inventions of many novel techniques and schemes, such as the flux corrected transport (FCT) algorithm (Boris and Book 1973, Book et al 1975) and its multidimensional extension by Zalesak (1979), the ultimate conservative difference schemes (Van Leer 1974, 1977, 1979), the flux limiters (Roe 1981 and Sweby 1984), the total variance diminishing (TVD) approach (Harten 1983), the multidimensional positive definite advection transport algorithm (MPDATA) (Smolarkiewicz 1984) and its monotonic version (Smolarkiewicz and Grabowski 1990), the essentially non-oscillation (ENO) scheme (Harten et al 1987), the universal limiters (Leonard 1991), the monotone area-preserving flux-form (MAPF) advection algorithm (Bott 1992), the weighted essentially non-oscillatory (WENO) scheme (Liu et al 1994), the multi-dimensional flux limiters (MFL) (Thuburn 1996), and so on. Most of these advanced schemes come with a price, that is, the increased computing cost. It is not a surprise that advection is one of the most expensive processes in many numerical models. Although computing power has

increased dramatically in the last few decades, demands for higher resolution, more physics and even coupled models have far outstripped the computer advance. For waves models the 2-D wave spectrum is represented by a huge mumber of discrete variables (over 20 directional bins and spectral bands on average leads to over 400 individual variables), which all need to be transported separately and result in a large advection computing task. It is hence still desirable to develop fast and robust advection schemes.

It is also arguable whether complex high-order advection schemes are necessary in models where physical diffusion or numerical smoothing is an essential process. The difference of non-oscillation advection schemes of different accuracy orders lies merely within their diffusion properties. The 1st order upstream scheme is notorious too diffusive and higher order schemes tend to reduce the numerical diffusion. However, the diffusion reduction in higher order schemes become trivial soon after the order is over 3rd (Leonard 1991). With a physical diffusion term in the same model, the improvement in advection scheme will effectively be wiped out by the real diffusion. Therefore, it should be enough to choose an advection scheme of numerical diffusion no larger than the real diffusion. The real diffusion could be reduced, if necessary, to compensate for the numerical diffusion incurred by the advection scheme. In fact, the diffusive 1st order upstream advection scheme is purposely selected for ocean wave models to smooth out the so called garden sprinkler effect caused by the discrete direction bins of the wave energy spectra (WAMDI group 1988). When less diffusive advection scheme is used, numerical smoothing has to be introduced to reduce this garden sprinkler effect (Tolman et al 2002). Hourdin and Armengaud (1999) demonstrated that higher-order schemes are much more accurate than lower order at a given spatial resolution but much more comparable when the lower-order schemes are run on a finer grid to make the numerical costs equivalent and suggested that a 2nd order non-oscillatory scheme is well suited for tracer transportation by 3-D atmospheric winds.

Irregular grids are commonly used in global atmospheric and oceanic models, such as the conventional longitude-latitude grid where the longitudinal grid spacing decreases with latitude. As Eulerian advection scheme is subject to the Courant-Friedrichs-Lewy (CFL) restriction, one direct consequence is the reduced time step due to the small longitudinal grid length near the polar regions. One solution to this problem is to increase the grid size in the polar regions such as the spherical reduced grid used by Rasch (1994), which doubles the longitudinal grid size gradually towards the poles so the actual grid spacing remains comparable to the equatorial one. The adaptive mesh refinement (Berger and Oliger 1984) and dynamic grid adaptation (Iselin et al 2002) attempt to accommodate the varying spatial and temporal scales of the atmospheric flow with different resolutions within one model. The multiple-cell grid (Li 2003) uses high resolution cells in interested area and gradually doubled cells in other areas to minimise memory usage. These adapted grids add extra difficulties in development of advection schemes.

This paper present two simple non-oscillatory advection schemes which may be used in wave models. The 2nd order scheme is highly recommended with the belief that higher accuracy may be achieved more conveniently by higher resolutions than by complicated schemes. The schemes will be presented in irregular grid formulation for possible wide applications in atmospheric and oceanic models. Classic 1-D and 2-D numerical tests on multiple-cell grids will be used for comparison with their classical counterparts and demonstration of their performance.

2. Upstream Non-Oscillatory (UNO) advection schemes

To find a cure for the numerical oscillation, it is best to start with the cause of the oscillation. The oscillation problem can be illustrated with the simple 1-D advection of a step function over a uniform grid. Assuming the step function is initially zero for all grid points up to cell j and jumps to 1 from cell j+1 onwards as shown in Fig. 1. The cause of oscillations in advection schemes can be directly linked to the evaluation of the j+1/2 face value between j and j+1 cells. Four simple 2nd order linear interpolation schemes are shown in Fig.1 to demonstrate this in addition to the 1st order upstream scheme and a quadratic interpolation scheme. The flow is assumed to be non-divergent. For 1-D case this requires the velocity to be a constant and it is assumed to be positive in Fig. 1.

The cell notation in Fig. 1 follows Leonard (1991). For each given cell face, j+1/2 with velocity $u_{j+1/2}$ for instance, a *Central* (C) cell is defined as the cell from which the flux cross the face comes (cell j when $u_{j+1/2} > 0$), which is also called the donor cell; The *Downstream* (D) cell is next to the central cell and receives the flux (cell j+1 when $u_{j+1/2} > 0$); and the other cell next to the central cell on the side opposite to the downstream cell is called the *Upstream* (U) cell (cell j-1 when $u_{j+1/2} > 0$). If the velocity is negative for the given j+1/2 face, the j+1 cell becomes the central cell, j the downstream cell and j+2 the upstream cell. All subsequent formulations will be given in this *Upstream-Central-Downstream* (UCD) notation.

To facilitate extension to multidimensional irregular grid with varied flow velocity, the grid coordinate x is assumed to be at the cell centre and the cell width Δx (always positive) may vary for non-uniform grid. So cell face will be half the cell width away from its cell centre but may not be at the middle point between the two

bounding cells in irregular grid. Finite difference will be based on cell centre coordinate and a gradient notation G_{AB} is defined between any two cell A and B as

$$G_{AB} \equiv (\psi_A - \psi_B)/(x_A - x_B) \tag{2}$$

which is symmetrical about the two points, that is, $G_{AB} = G_{BA}$.

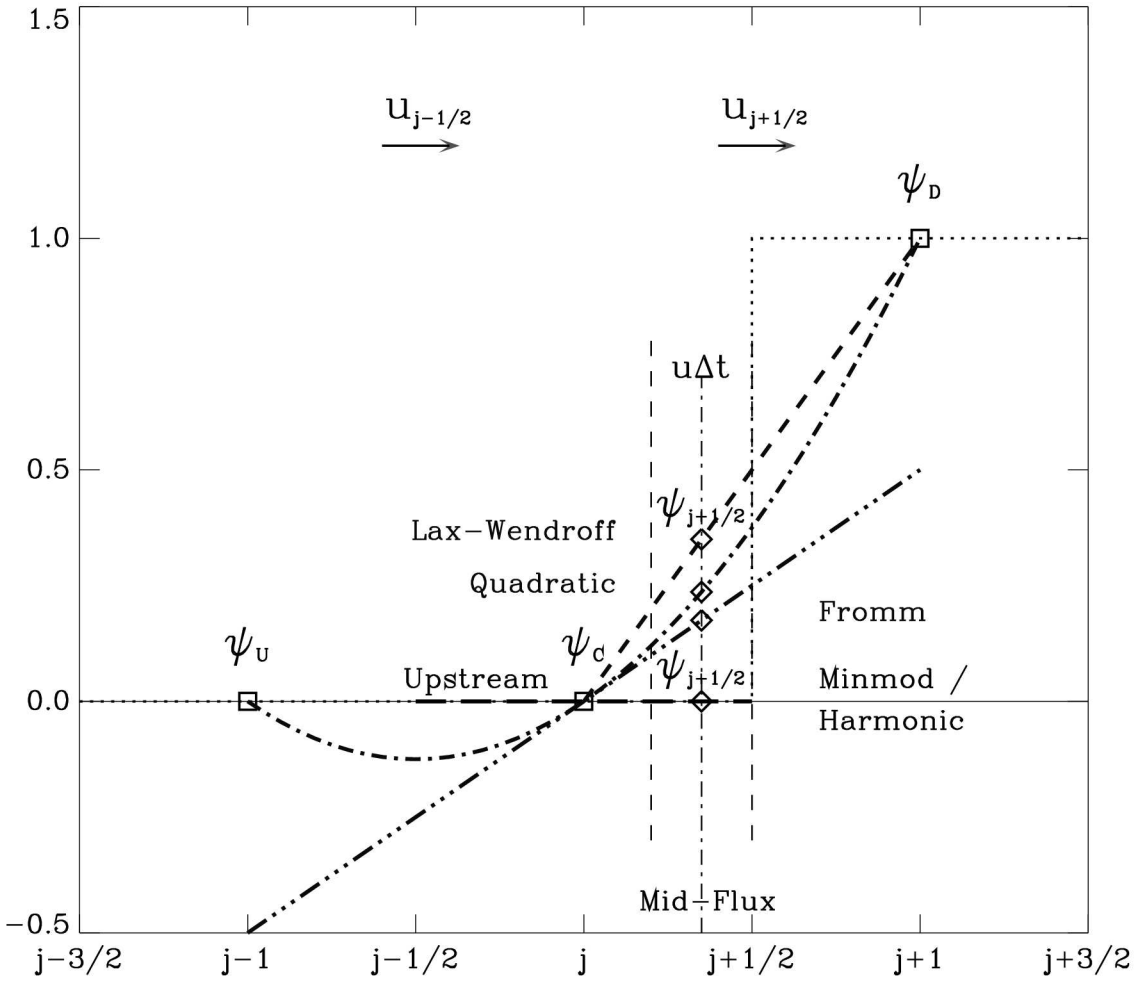

Fig. 1. Interpolation of a step function by 6 different advection schemes.

Noticing the fact that when Courant number $\mu = u\Delta t/\Delta x$ equal to 1 the advection simply moves the whole central cell content into the downstream cell in one time step Δt. This is exactly what the 1st order upstream scheme does. It is then essential for higher order schemes to revert to the 1st order upstream scheme when the Courant number approaches 1. For interpolation schemes, this may be achieved by using the interpolation value at the *Mid-Flux* (MF) point x_{MF}, or $|u|\Delta t/2$ upstream from the cell face or $(\Delta x - |u|\Delta t)/2$ downstream from the donor cell centre. The linearly interpolated MF value for flux crossing the $j+1/2$ face is then given by:

$$\begin{aligned} \psi^{MF}_{j+1/2} &= \psi^n_C + (x_{MF} - x_C) G_C \\ x_{MF} &= x_C + sign(u_{j+1/2})(\Delta x_C - |u_{j+1/2}|\Delta t)/2 \end{aligned} \tag{3}$$

Where $\psi^n{}_C$ is the central (or donor) cell value at time level n in relative to the $j+1/2$ face velocity $u_{j+1/2}$ and G_C the selected gradient for the central cell. It is obvious that the interpolated value will be equal to the central cell value when the Courant number approaches unity no matter what central gradient is used in (3). The updated cell j value will be given in the conservative flux-form as

$$\psi_j^{n+1} = \psi_j^n + \left(u_{j-1/2}\psi_{j-1/2}^{MF} - u_{j+1/2}\psi_{j+1/2}^{MF}\right)\Delta t/\Delta x_j \tag{4}$$

The MF point interpolation (3) also guarantees that the forward-in-time update (4) is 2nd order accurate in time.

All the four linear interpolation schemes shown in Fig.1 use the MF values but with different central cell gradients. The 1st order upstream scheme is given by simply setting $G_C = 0$. As central cell j value is zero here, the outward flux from cell j is simply zero. Because the input flux to cell j from the upstream cell j-1 is also zero by the upstream scheme, the net increment for cell j is zero or cell j content will be left unchanged by the upstream scheme. This is part of the reason why the upstream scheme is free from oscillation.

For the 2nd order Lax-Wendroff scheme, the face value is evaluated as the linear interpolation between the central and downstream cells, which is equivalent to using a gradient $G_C = G_{DC}$ in (3). The interpolated MF value for the step function in Fig. 1 is obviously non-zero when $\mu < 1$ as the cell value jumps from 0 at cell j to 1 in cell j+1. The flux entering cell j from the left cell face j-1/2 will be zero by the Lax-Wendroff scheme, resulting in a net non-zero flux out of cell j. This non-zero net flux out of an empty cell j makes the updated cell j value to be negative and hence stirs up a trailing oscillation for the Lax-Wendroff scheme.

The Fromm (1968) scheme (though derived from a different approach) is equivalent to using the centred gradient of the central cell for interpolation of the MF value, that is, $G_C = G_{DU}$. It results in a reduced but still non-zero MF value as shown in Fig.1. The left-side flux for cell j is also zero by the Fromm scheme and hence the net flux out of cell j is non-zero again though it is smaller than the Lax-Wendroff one. So the oscillation is alleviated in comparison with the Lax-Wendroff scheme but not completely eliminated by the Fromm scheme.

Roe (1985) introduced a simple but efficient way to remove the oscillations by choosing one gradient of minimum modulus (hence called *minmod* scheme) among the two side gradients (G_{DC} and G_{CU}) if the central cell value is between the upstream and downstream cell values or within the monotonic region defined by $G_{DC}G_{CU} > 0$. Outside the monotonic region, the gradient is simply set to be zero, which is equivalent to reverting to the 1st order upstream scheme. Because the side gradient between cell j-1 and j is zero in the step function case in Fig.1, the selected gradient is effectively zero and hence the MF value is equal to the cell j value. So the minmod scheme leads to a net zero flux for cell j and keeps it unchanged in the update.

The minmod scheme can be further simplified as it is not necessary to restrict the minmod gradient within the monotonic region as long as the sign of local side gradient G_{DC} is used. This extension is shape-preserving under the CFL condition which restricts the MF point within the central cell between the cell centre and its downstream cell face. The simplified minmod scheme led to the following central cell gradient in the UCD notation:

UNO2: $$G_C = Sign\left(G_{DC}\right)\min\left(\left|G_{DC}\right|,\left|G_{CU}\right|\right) \tag{5}$$

This simplified 2nd order scheme will be referred to as UNO2 scheme. Inserting (5) into (3) yields the MF value of the UNO2 scheme. Noticing that the sign of the velocity is cancelled with the sign of the grid difference ($x_D - x_C$), the product of the local gradient sign with the face velocity sign in (3) becomes a single sign function of the cell difference ($\psi_D - \psi_C$). Besides, there is no need to compare the signs of the two side gradients in UNO2. Hence only one sign function of the cell difference is needed in the UNO2 MF value interpolation. This sign optimisation may benefit in computer code by directly calculating the absolute gradient for each face once in one loop. The MF value is then given by the minimum absolute gradient and the merged sign of the cell difference ($\psi_D - \psi_C$):

UNO2: $$\psi_{j+1/2}^{MF} = \psi_C^n + 0.5sign\left(\psi_D^n - \psi_C^n\right)\left(\Delta x_C - \left|u_{j+1/2}\right|\Delta t\right)\min\left(\left|G_{DC}\right|,\left|G_{CU}\right|\right)$$

As the FORTRAN sign function is effectively a sign transfer function, the 0.5 factor can be absorbed into the FORTRAN sign function (that is, SIGN(0.5, $\psi_D - \psi_C$) in FORTRAN code) to reduce one more multiplication. The UNO2 scheme differs from the minmod scheme only when the central cell is at a peak ($\psi_C > \psi_U, \psi_D$) or a dip ($\psi_C < \psi_U, \psi_D$) point. The UNO2 scheme will only smooth back the peak or dip point for a non-divergent flow and hence will preserve the non-oscillation property of the minmod scheme. The optimised UNO2 scheme is the simplest 2nd order non-oscillatory scheme as far as the author knows.

The van Leer (1977) harmonic scheme, which uses the harmonic average of the two side gradients within the monotonic region, is also free from oscillation and has even better performance than the minmod scheme. The harmonic average becomes zero if any one of the two side gradients is zero. For the step function case in Fig.1, it becomes zero for the j cell as the upstream side gradient is zero. So the cell j value is kept unchanged in the harmonic scheme update just like the upstream and minmod schemes. The harmonic average, however, is invalid outside the monotonic region where the two gradients are of opposite signs. The harmonic scheme

reverts to the 1st order scheme outside the monotonic region for this reason. Based on the same argument for minmod scheme, the harmonic scheme may be extended outside the monotonic region by using the harmonic average of absolute side gradients and the local gradient sign, resulting in the following modified absolute harmonic scheme:

$$\text{UNO2}^+: \qquad G_C = Sign(G_{DC})\,2|G_{DC}G_{CU}|/\left(|G_{DC}|+|G_{CU}|+\varepsilon\right) \tag{6}$$

which will be referred to as UNO2$^+$ scheme as it is slightly better than the UNO2 scheme. Note that a small positive value ε is added to the denominator in the absolute harmonic average to avoid zero-dividing. It may be chosen close to the minimum real value for a given computer (for example, $\varepsilon = 10^{-30}$ on a 32-bit machine) so that it has virtually no effect on the averaged gradient. Similar to the UNO2 scheme, the UNO2$^+$ scheme can be optimised by calculating the absolute side gradient for each cell face once in one loop and using the merged sign in the MF value interpolation with the absolute harmonic average:

$$\text{UNO2}^+: \qquad \psi^{MF}_{j+1/2} = \psi^n_C + sign\left(\psi^n_D - \psi^n_C\right)\left(\Delta x_C - \left|u_{j+1/2}\right|\Delta t\right)|G_{DC}G_{CU}|/\left(|G_{DC}|+|G_{CU}|+\varepsilon\right)$$

The UNO2$^+$ scheme has very similar performance and computing cost as the harmonic scheme. So the modification is of more theoretical value than performance gain here. Nevertheless, UNO2$^+$ has eliminated the sign comparison used in the harmonic scheme to make the coding more friendly to vectorization.

Using upstream biased four grid points for each cell update, Takacs (1985) derived an advection scheme of 3rd order accuracy in both time and space. It is equivalent to use the UCD cells for each flux evaluation. The scheme can be extended to irregular grid and the equivalent central cell gradient for MF value interpolation is given in the UCD notation as:

$$3^{\text{rd}}: \qquad G_C = G_{DC} - \frac{4\left(x_D - x_{MF}\right)}{3}\left(\frac{G_{DC} - G_{CU}}{x_D - x_U}\right) \tag{7}$$

Note that $|x_D - x_{MF}| = (\Delta x_D + |u_{j+1/2}|\Delta t)/2$ is complement to $(\Delta x_C - |u_{j+1/2}|\Delta t)/2$ for the distance between the central and downstream cells. The scheme is exactly 3rd order accurate in time and space for uniform grid with constant velocity (Takacs 1985, Leonard 1991). The quadratic interpolation using the UCD cells for the j+1/2 MF value leads to a central cell gradient similar to the 3rd order one (7) except that the numerical denominator 3 is replaced by 4. However, the quadratic interpolation scheme is only 2nd order accurate in time. It is not very difficult to prove that both the 3rd order and quadratic schemes lead to non-zero fluxes out of cell j for the step function case shown in Fig.1. As long as the Courant number is less than one, they will generate oscillations as well.

It may be generalised that any interpolation based on continuous functions (such as polynomials) will result in non-zero flux for this step function shown in Fig. 1 and hence cause oscillation no matter how high the order of accuracy is attempted. This explains why all the high-order schemes given by Tremback et al (1987) resulted in oscillations. Other interpolation approaches, such as the piecewise parabolic method (PPM) (Colella and Woodward 1984), the second-order moments (SOM) conservation (Prather 1986), the second-degree Chebyshev polynomial interpolation (Holm 1995), and the dual-linear sub-grid approximation (Walcek and Aleksic 1998), also result in oscillations and have to resort to flux limiters or flux correction to remove them. It is then necessary for any non-oscillatory scheme to produce a net flux out of cell j to be zero in this step function case in order to keep the cell j value unchanged. This is achieved by the upstream, minimod and harmonic schemes by reducing the central cell gradient to be zero for j+1/2 face MF value interpolation. Other non-oscillatory schemes, such as TVD and flux limiters, though based on slightly different concepts, all lead to mathematically equivalent local bounding schemes (Thuburn 1997) and result in a net zero flux out of cell j in the step function case in Fig. 1. The ENO scheme is virtually the same as the minmod scheme for this special case. The PPM scheme reverts to constant sub-grid function for cell j and hence is equivalent to the upstream scheme in this case. The MAPF and MFL schemes modify input or output flux so that net flux of cell j is zero in this step function case. Proofs of these statements are omitted here and interested readers may refer to the original papers of these advanced schemes.

Leonard (1991) combined the 3rd order scheme (7) with the so called ULTIMATE flux limiters and resulted in a non-oscillation scheme called the ULTIMATE QUICKEST scheme. One important conclusion of this scheme is that the 3rd order scheme is used *without* any modification within a limited monotonic zone, which may be defined in irregular grid by

$$\left|G_{DC} - G_{CU}\right| \le 1.2\left|G_{DU}\right| \tag{8}$$

Outside this limited zone but still inside the monotonic region, flux limiters are used to modify the 3rd order flux value. It reverts to the 1st order upstream scheme outside the monotonic region. One drawback of the ULTIMATE strategy is that the Courant number is used as a denominator in one of its limiters. As the Courant number may become zero in multi-dimensional flow, it may generate an unnecessary large limiter even if a minimal number might be added to avoid zero-dividing. Besides, flux limiters are also more expensive than direct formulation as they involve extra conditional checks on flux values which do not favour vectorization and parallelisation. These flux limiters might be avoided if other direct formulation, such as the UNO2$^+$ scheme, is used outside the limited monotonic zone. This leads to the following simplified 3rd order scheme and it will be referred to as UNO3$^-$ scheme:

$$\text{UNO3}^-\text{:}\quad \begin{aligned} & G_C = G_{DC} - \frac{4\left(x_D - x_{MF}\right)}{3}\left(\frac{G_{DC} - G_{CU}}{x_D - x_U}\right) \qquad for \quad \left|G_{DC} - G_{CU}\right| \le 1.2\left|G_{DU}\right|; \\ & Otherwise \quad G_C = Sign\left(G_{DC}\right) 2\left|G_{DC} G_{CU}\right| / \left(\left|G_{DC}\right| + \left|G_{CU}\right| + \varepsilon\right) \end{aligned} \tag{9}$$

One minor flaw in the UNO3$^-$ scheme is that the flux value has a small jump at the switching point from the 3rd order scheme to UNO2$^+$ scheme. This discontinuity might be even larger if the UNO2 scheme is used outside the limited monotonic zone. However, the gap at the switching point can be reduced by doubling the minmod gradient within the monotonic region, resulting in the following improved 3rd order scheme, which will be referred to as UNO3:

$$\text{UNO3:}\quad \begin{aligned} & G_C = G_{DC} - \frac{4\left(x_D - x_{MF}\right)}{3}\left(\frac{G_{DC} - G_{CU}}{x_D - x_U}\right) \qquad for \left|G_{DC} - G_{CU}\right| \le 1.2\left|G_{DU}\right|; \\ & Else \quad G_C = 2Sign\left(G_{DC}\right)\min\left(\left|G_{DC}\right|, \left|G_{CU}\right|\right) \qquad for\ G_{DC} G_{CU} > 0 \\ & Otherwise \quad G_C = Sign\left(G_{DC}\right)\min\left(\left|G_{DC}\right|, \left|G_{CU}\right|\right) \end{aligned} \tag{10}$$

The doubling factor 2 for the UNO2 scheme inside the monotonic zone is the maximum value allowed so that the enhanced UNO2 value does not exceed the 3rd order value at the switching point. The switching from the doubled UNO2 gradient to the UNO2 one on the monotonic edge is continuous as the UNO2 gradient is zero there. Back to the step function case in Fig. 1, as the central cell value is on the edge of the monotonic region, both the UNO3$^-$ and UNO3 schemes effectively produce a zero central cell gradient for the j+1/2 MF value interpolation. So both schemes will not change the cell j value in their updates as other non-oscillatory schemes.

Extending the 1-D UNO schemes to 2-D is straightforward by applying the 1-D scheme simultaneously to each of the two dimensions before updating the next time level values. The drawback of this direct or simultaneous implementation is that the Courant number in the stable condition, $|\mu| < 1.0$, has to be replaced by the absolute sum of all component Courant numbers, that is, $|\mu|+|\nu| < 1.0$, where $\nu=\upsilon\Delta t/\Delta y$ is the Courant number and the υ the velocity component for the y dimension. If the 1-D scheme is applied in sequence or by time-splitting approach, the stable condition may be relaxed to each component one, $\max(|\mu|, |\nu|) < 1.0$. However, it results in the so called time-splitting error which typically distorts a constant background into a non-constant field in deforming flow. Leonard et al (1996) constructed a multi-dimensional advective-conservative hybrid operator (MACHO) to extend 1-D advection scheme to 2-D with preserved constancy. The operator is similar to the time-splitting approach except that the MF value for the second dimension ψ^{*MF} is calculated with a temporary advective-form update ψ^* of the 1st dimension using cell centre velocity,

$$\psi^*_{i,j} = \psi^n_{i,j} + \left(\psi^{MF}_{i-1/2,j} - \psi^{MF}_{i+1/2,j}\right)\left(u_{i-1/2,j} + u_{i+1/2,j}\right)\Delta t / 2\Delta x_i \tag{11}$$

The final update of cell (i,j) value still uses the conservative-form for both dimensions:

$$\begin{aligned} \psi^{n+1}_{i,j} = \psi^n_{i,j} & + \left(u_{i-1/2,j}\psi^{MF}_{i-1/2,j} - u_{i+1/2,j}\psi^{MF}_{i+1/2,j}\right)\Delta t / \Delta x_i \\ & + \left(\upsilon_{i,j-1/2}\psi^{*MF}_{i,j-1/2} - \upsilon_{i,j+1/2}\psi^{*MF}_{i,j+1/2}\right)\Delta t / \Delta y_j \end{aligned} \tag{12}$$

The temporary advective-form update (11) ensures a constant field remains constant and hence the MF values for both dimensions are interpolated from the same constant field. As long as the non-divergence condition is satisfied for each cell volume a constant field updated by (12) will remain constant. Because the operator is

asymmetrical, the dimensions are alternated in sequence between time steps, that is, for the next time step, the second dimension MF values are calculated first and its advective-form update is used for the interpolation of the first dimension MF values. The stability condition for the MACHO update (12) remains the component one.

The UNO schemes are consistent, that is, they converge to the continuous advection equation (1) when Δx and Δt approaches zero. Proof of the consistency is straightforward as all the four UNO schemes are based on cell gradients. They are also conservative due to their conservative formulations. Positive-definite is automatically guaranteed by their shape-preserving property in any non-divergent flow for any positive field, like the wave enery spectrum. Nevertheless, positive filter is recommended for wave spectral models as non-divergent condition may not be satisfied for some boundary cells in wave models.

3. One-dimensional tests

As most of the classical advection schemes are presented in 1-D uniform grid formulation, comparisons of the UNO schemes with their classical counterparts are carried out in 1-D uniform grid test as shown in Fig.2. The flow is assumed non-divergent or of constant velocity. Cyclic boundary condition is used to facilitate arbitrary modelling time with the 500 cells. The initial profile consists of a cone and a step pulse as shown by the thin lines in all the panels in Fig.2. The Courant number is set to be 0.625 so that a full cycle over the 500 cells takes exactly 800 steps. Because half of the UNO2 scheme is equivalent to the Lax-Wendroff scheme, the Courant number is deliberately chosen to be less than $1/\sqrt{2}$ when the phase velocity of the Lax-Wendroff scheme reverses sign for short waves. All the results in Fig. 2 are after 4 complete cycles or 3200 time steps.

Panel (a) in Fig. 2 shows the results by the 1st order upstream scheme, which is included here as a reference for other schemes. After 3200 time steps, both the initial cone and the step pulse (shown by the thin solid line) are changed into smooth cones without any sharp point (thick line) by the upstream advection scheme. The rms error between the initial and the final profile over the 500 cell points is 0.1859.

Panel (b) and (c) in Fig. 2 show the UNO2 and minmod results, respectively. They are no difference at all and both share the same rms error of 0.0842. So the UNO2 extension of the minmod scheme beyond the monotonic region has no visible effect on the final results. These results are not surprising as the UNO2 and minmod schemes only differ at peak and dip points. The numerical smoothing, however, effectively round off these points and reduced the gradients around these points close to zero. Hence the two schemes become effectively the same for the smoothed field. This is also true for the UNO2$^+$ extension of the harmonic scheme as shown in panel (d) and (e). The two schemes share the same rms error of 0.0639, which is smaller than the minmod and UNO2 error.

The 3rd order ULTIMATE QUICKEST result is shown in panel (g) which has the minimum rms error (0.0583) among all the schemes shown in Fig.2. The UNO3$^-$ and UNO3 schemes are shown in panel (f) and (h). The rms errors by these two schemes are 0.587 and 0.586, respectively, which are slightly larger than the ULTIMATE QUICKEST one. Considering the simplification of removing all flux limiters in the UNO3$^-$ and UNO3 schemes, this small loss of accuracy is worthwhile.

It is obvious that all the schemes shown in Fig. 2 are free from oscillations. Numerical results confirm that all cell values remain non-negative (minimum to be 0 in 64 bit double precision) for all the 3200 time steps without using any filter. So the UNO schemes will automatically be positive-definite for positive tracer transportation.

One-dimensional multiple-cell grid is used to test the irregular formulation of the UNO schemes. The multiple-cell grid is the same as the previous 500-cell uniform grid except that each of the central 100 cells is divided into 2 cells to form a high resolution section. This grid is similar to the multiple-cell grid used by Li (2003) except that here it is for 1-D only. The time step is halved to keep the Courant number in the high resolution part to be the same as in the uniform grid test (0.625). The Courant number is halved in the outskirts or low resolution part (0.3125) as the cell width is doubled. One full cycle over these 600-cell irregular grids takes exactly 1600 time steps. Fig. 3 shows the results for the upstream, UNO2 and UNO3 schemes after 3200 (thick solid line) and 25600 (dot-dashed line) time steps, respectively.

The initial profile as shown by the thin solid line in Fig. 3 is different from the one used in the uniform grid test (see Fig. 2). The new profile consists of one extended step pulse (from -150 to 150) with a sine shaped slope in the high resolution part (from -50 to 50), connected by two linear slopes to the step pulse. The new profile has a dip and a peak at the ends of the sine slope to test the UNO schemes outside the monotonic region. The results clearly reveal that the UNO schemes smooth back the peak and dip points just as the 1st order upstream scheme except that the smoothing by the UNO schemes is much localised around discontinuous gradient points. In fact, the UNO scheme smoothing is self-limiting and vanishes quickly as the advected profile becomes smooth. Allen et al (1991) mentioned this self-limiting diffusion in the van Leer harmonic scheme and used a cyclic triangle advection to illustrate it. This difference may be revealed here by comparing the results after 2 cycles (or 3200 time steps) with the results after 16 cycles (or 25600 time steps) in Fig. 3. The upstream

scheme smoothed out all features of the initial profile after 25600 time steps, leaving a single raised bump. The UNO2 scheme managed to keep the essential features of the initial profile though the flat parts of the step pulse were lost. The UNO3 scheme preserved all the features of the initial profile except that the discontinuous gradient points have been smoothed out. The profile after 16 cycles (rms = 0.0677) has very small difference from the one after 2 cycles (rms = 0.0516). This self-restrained diffusion will have very small effect on continuous variables and hence the UNO3 scheme may be used for advection with very small diffusion, like tracer transportation in the deep ocean (Li et al 2003).

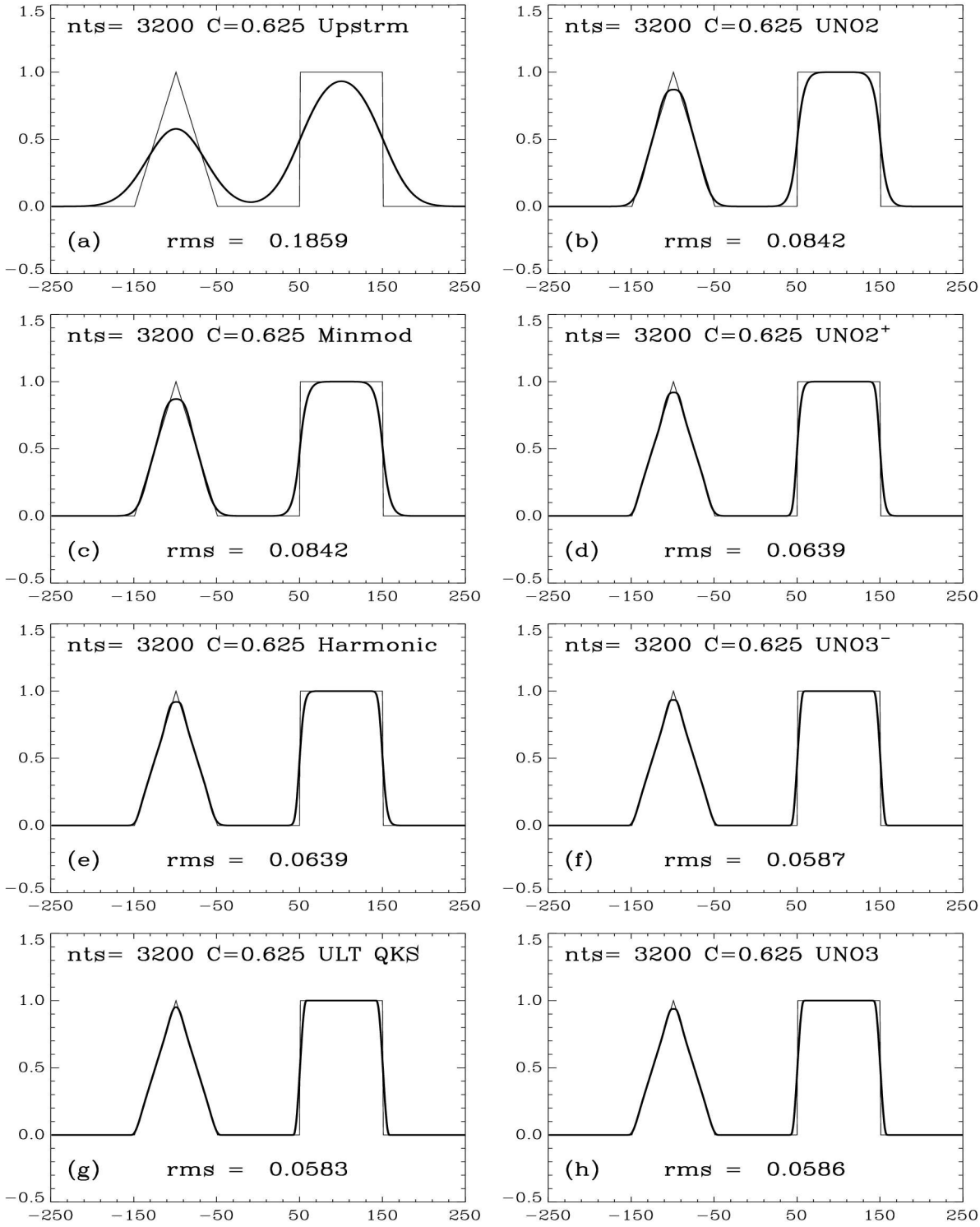

Fig. 2. Comparison of classical and UNO advection schemes.

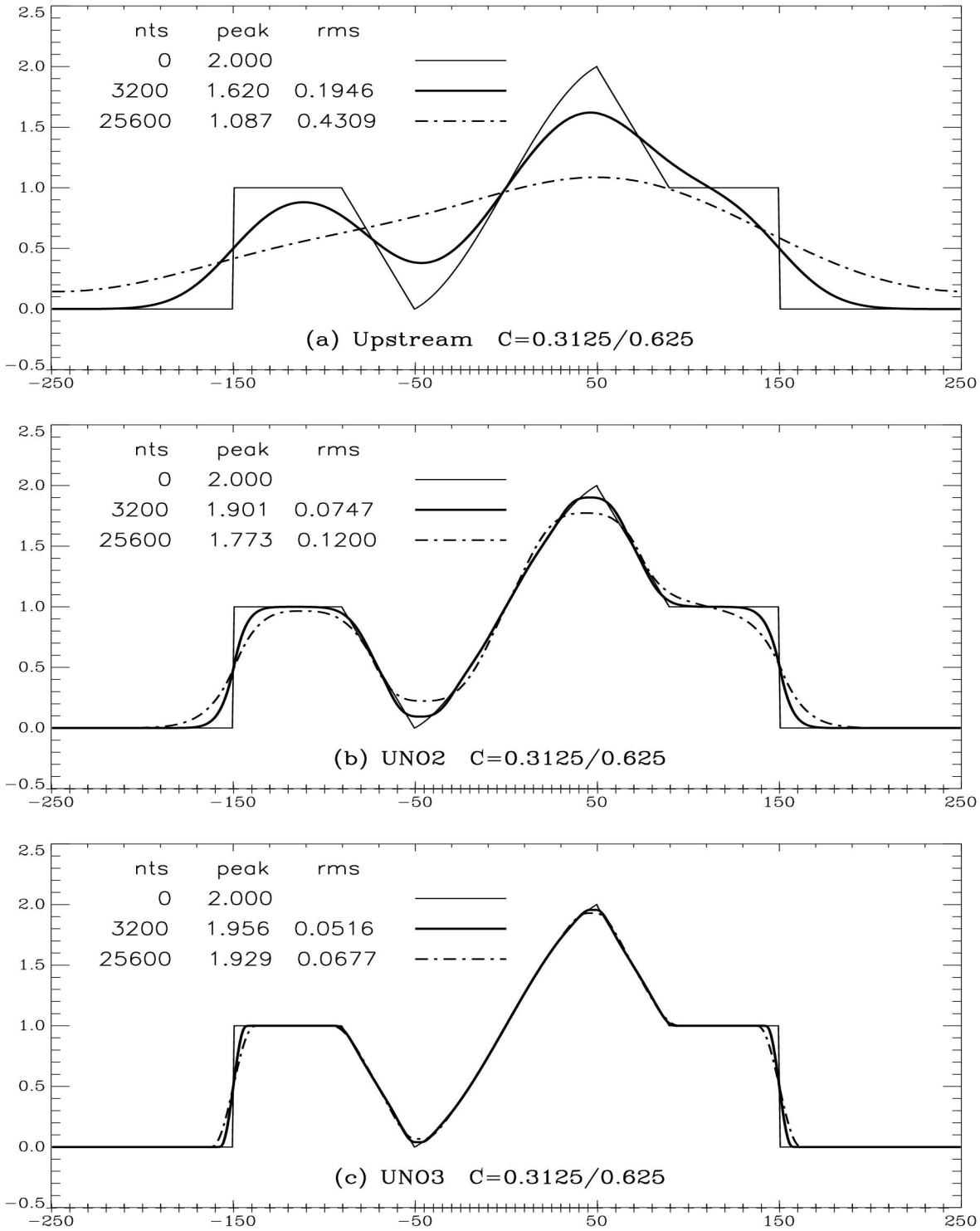

Fig. 3. Comparison of upstream and UNO schemes in 1-D multiple cell grid test.

The UNO2 scheme is the simplest 2nd order non-oscillatory scheme among all non-oscillatory schemes found in the literature and will be useful for advection and diffusion process, like the tracer transportation in the atmospheric boundary layer where the physical diffusion is present and numerical smoothing is also required (Davies et al 2005). The simplicity and reliability of the UNO2 scheme will be valuable for environmental models when many species have to be simulated. It may also be used in ocean wave spectral models where moderate smoothing is required to reduce the garden sprinkler effect on the discretised energy spectrum of the ocean surface wave (Tolman et al 2002).

4. Two-dimensional tests

Two classical 2-D numerical tests for advection schemes are applied on the UNO schemes. The first one is the solid rotation experiment and the other is the Smolarkiewicz (1982) deformation test. These tests are carried out on a 2-D multiple-cell grid (Li 2003) as shown in Fig. 4. The central test bed is a square area consisting of 104 by 104 size 1 (Δx by Δy) cells. Eight layers of size 2 ($2\Delta x$ by $2\Delta y$) cells are laid around the central area and further away are four layers of size 4 ($4\Delta x$ by $4\Delta y$) cells. All cells are square ($\Delta x = \Delta y$) to meet the non-divergent requirement of the deformation flow though the cell sizes may change. The multiple-cell grid is different from the conventional 2-D grid for its arbitrary cell arrangement. To demonstrate this flexibility, cells on the four corners have been removed if they are 88 basic cell lengths away from the model centre. These redundant corner cells would not have much effect on the central test area in both the rotation and deformation tests if they were included. The remaining cells are arranged in arbitrary sequence in a preset cell array, which contains cell position and size information and is used for cell-related calculation. The numbers inside the size 4 cells in Fig. 4 indicate the sequence numbers of the 344 size 4 cells used in these tests. Cell faces are grouped by their normal velocity components and two (u- and v-) face arrays are used to store face position, size, and its bounding cell numbers for each face. These face arrays are used for calculation of MF values or fluxes crossing the cell faces. To facilitate the UCD interpolation of MF values, these face arrays are expanded in this study to contain the 2 immediate cells on both sides of each cell face. Each boundary cell face is assumed to be bounded by two boundary cells of the same size as the face on the outside. This allows that all cell faces to be treated the same way no matter whether they are inner faces or boundary faces and that boundary conditions can be applied by modifying these boundary cell values. For the two tests here the boundary cells are assumed to be constantly empty, that is, no flux comes into the model domain and outward flux crossing the boundary face will disappear immediately. Details of the multiple-cell grid are available from Li (2003). The multiple-cell grid is similar to the adaptive mesh refinement (Berger and Oliger 1984) except that the different resolution parts are preset and remain unchanged during the tests. It may be converted into the spherical reduced grid (Rasch 1994) by doubling only the longitude dimension at high latitudes.

In the 2-D solid rotation test, the velocity field is specified to rotate around the centre of the model domain and one full rotation takes exactly 480 time steps. The maximum Courant number on the edge of the central size 1 area is $104\pi/480 \sim 0.681$. Note that the Courant number is halved when the cell size is doubled in the size 2 area so the Courant number outside the central size 1 area will be less than the central edge value. A Gaussian cone (5 units high at peak) is initially placed in the lower-left quarter of the central area above a uniform non-zero (1 unit high) background as shown in the upper panel of Fig. 5. Note that the multiple-cell field has been converted into a uniform square domain of size 1 cell resolution for the mesh plot. Each size 2 cell is presented by 4 equal size 1 grids and each size 4 cell by 16 equal size 1 grids in the mesh plot. The removed corner parts are set to be zero. The different cell sizes around the boundary are revealed by the difference between the 1-unit high uniform background and the zero outside points.

A perfect advection scheme would restore the original cone after one complete rotation. Unfortunately, such a perfect advection scheme has not been invented yet. The difference between the initial and the rotated cone, then, reveals how close the advection scheme is to a perfect one. The lower panel in Fig. 5 shows the result by UNO3 scheme after 1 full rotation or 480 steps. The different cell sizes are now indicated by the steps leading to the boundary. The uniform background in the central area remains uniform without any ripples even in the cell size changing region, implying that the irregular grid formulation of the UNO3 scheme works fine in the multiple-cell grid. Because fluxes out of boundary faces are lost the uniform background near the boundary was transformed into a smooth slope without any oscillations. The rotated cone preserved its initial shape quite well with its height reduced by nearly 1 unit out of 5 in 480 time steps.

For comparison purpose, the rotation results by the upstream and UNO2 schemes are shown in Fig. 9. The diffusive upstream scheme (upper panel in Fig. 9) reduced the initial 5-unit high cone to a flat bump of height less than 1 unit in 480 time steps. The leak from the boundary faces are also quicker than that by the UNO3 scheme, resulting in a gentle slope extended into the central size 1 area. The UNO2 scheme (lower panel in Fig. 9) scored a mark between those of the UNO3 and upstream schemes as expected. It managed to keep over half of the initial cone height (2.68 out of 5 units) after one rotation and maintained the central background uniform. Performance of the $UNO2^+$ and the $UNO3^-$ schemes are between the UNO2 and UNO3 schemes as their names indicate but their results are not shown here.

Smolarkiewicz (1982) introduced a deformation flow to test advection schemes and this deformation test was adopted by other authors (such as Bott, 1993; Lenonard et al., 1996). The 2-D velocity field of this deformation flow is given by

$$u(x,y) = u_0 \sin(kx)\sin(ky)$$
$$v(x,y) = u_0 \cos(kx)\cos(ky)$$

where u_0 is the wind speed on vertex edges, $k = \pi/26\Delta x$ is a constant wave number. The vertex size is slightly modified from the original one (Smolarkiewicz 1982) so that all vertex edges fall on cell faces (exactly 26x26 size 1 cells in each vertex) except in the size 4 cell area. The wind field is non-divergent for each cell as long as the cell is square. The multiple-cell grid is set to be square for this purpose. The time step and u_0 are chosen so that the maximum Courant number, $u_0\Delta t/\Delta x$, is of the same value 0.7 as used by other authors (such as Smolarkiewicz, 1982; Bott, 1993).

Staniforth et al. (1987) presented an exact solution of this deformation flow, which is characterised by two regimes: short time periods when t is about the order of $T = 2\pi/ku_0$ (or about 75 time steps in this configuration) and long time periods when $t >> T$. In the first regime, numerical solutions using finite difference schemes may be compared with the exact solution in a quantitative manner. In the second regime, however, the exact solution has too much short-scale information which is beyond the practical resolution of any finite difference method. Numerical solutions should be evaluated, in the latter regime, on the basis of stability and a qualitative similarity with an appropriate averaging of the exact solution, which resembles an egg-cup over each of the two central vortices and has the strongest gradients at vortex boundaries, where the solution becomes almost vertical. A few classical schemes (such as the 2nd order Lax-Wendroff scheme and the 3rd order Gadd (1978) scheme) passed the first regime without much problem but failed to produce the egg-shaped average field in the second regime.

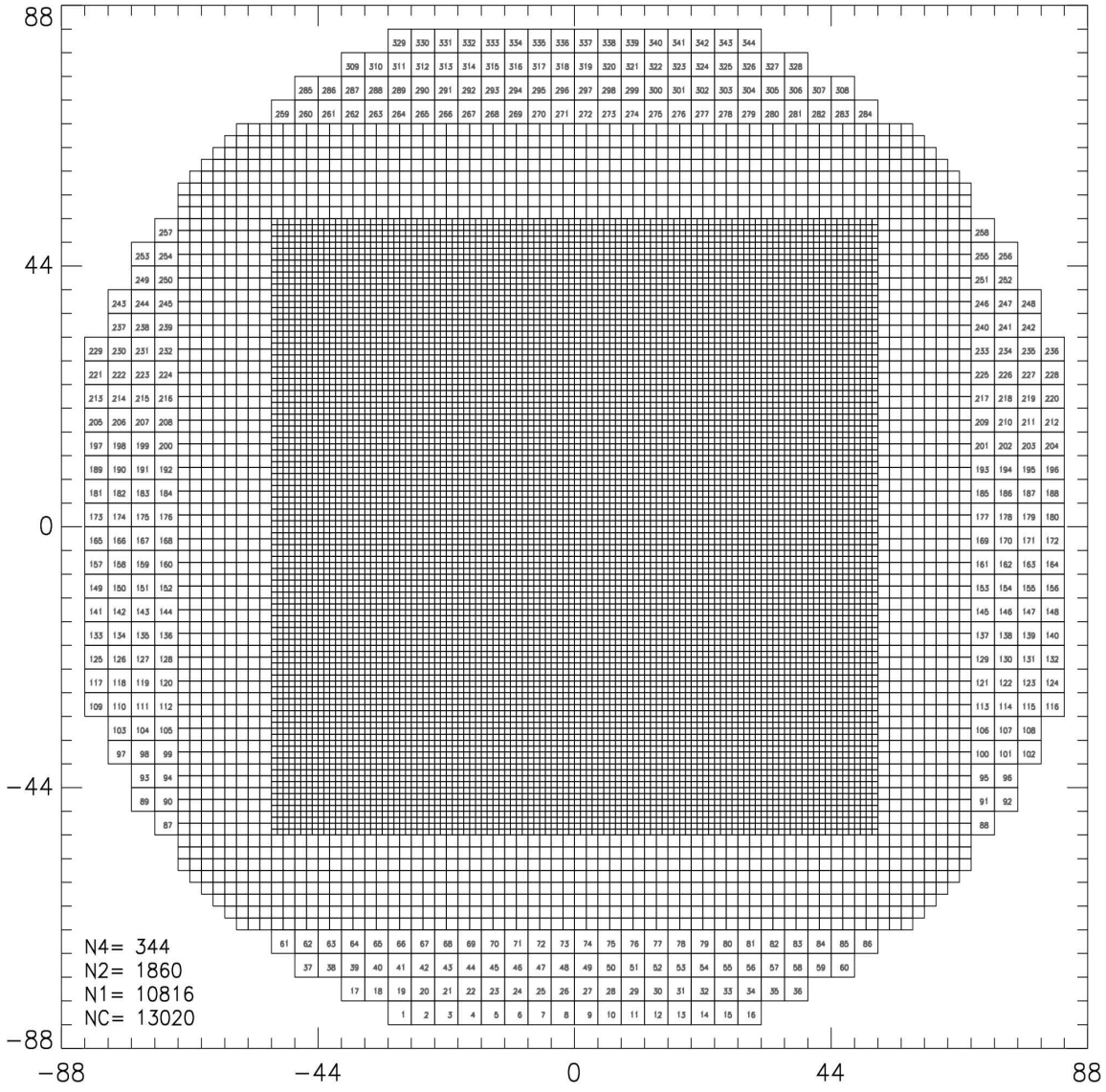

Fig.4. Multiple-cell grid used for 2-D rotation and deformation tests.

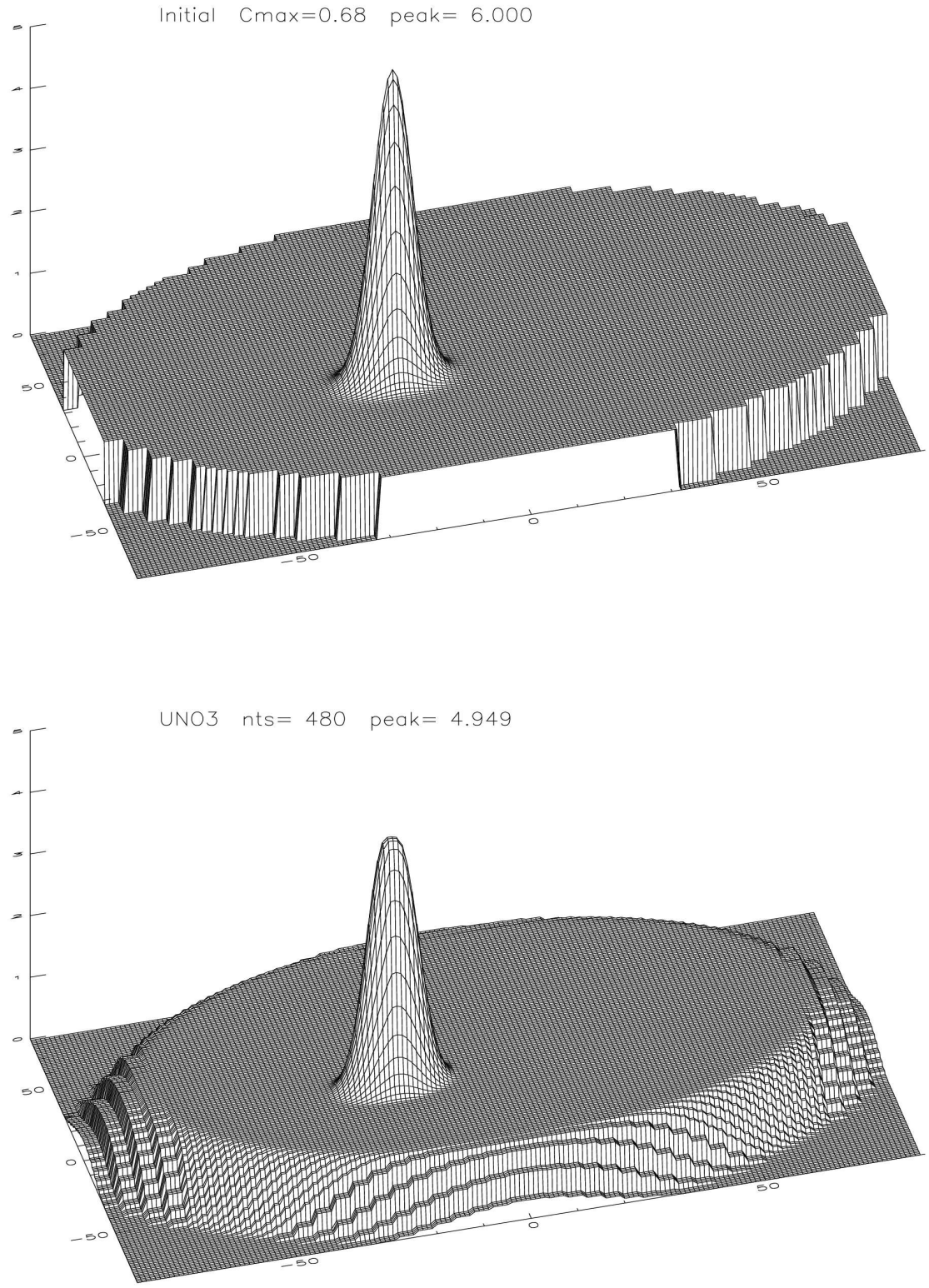

Fig. 5. Solid roation test of the UNO3 scheme. Upper panel shows the intial Gaussian cone and the uniform background over the full multiple-cell grid. Lower panel is the result by UNO3 scheme after 1 rotation or 480 time steps.

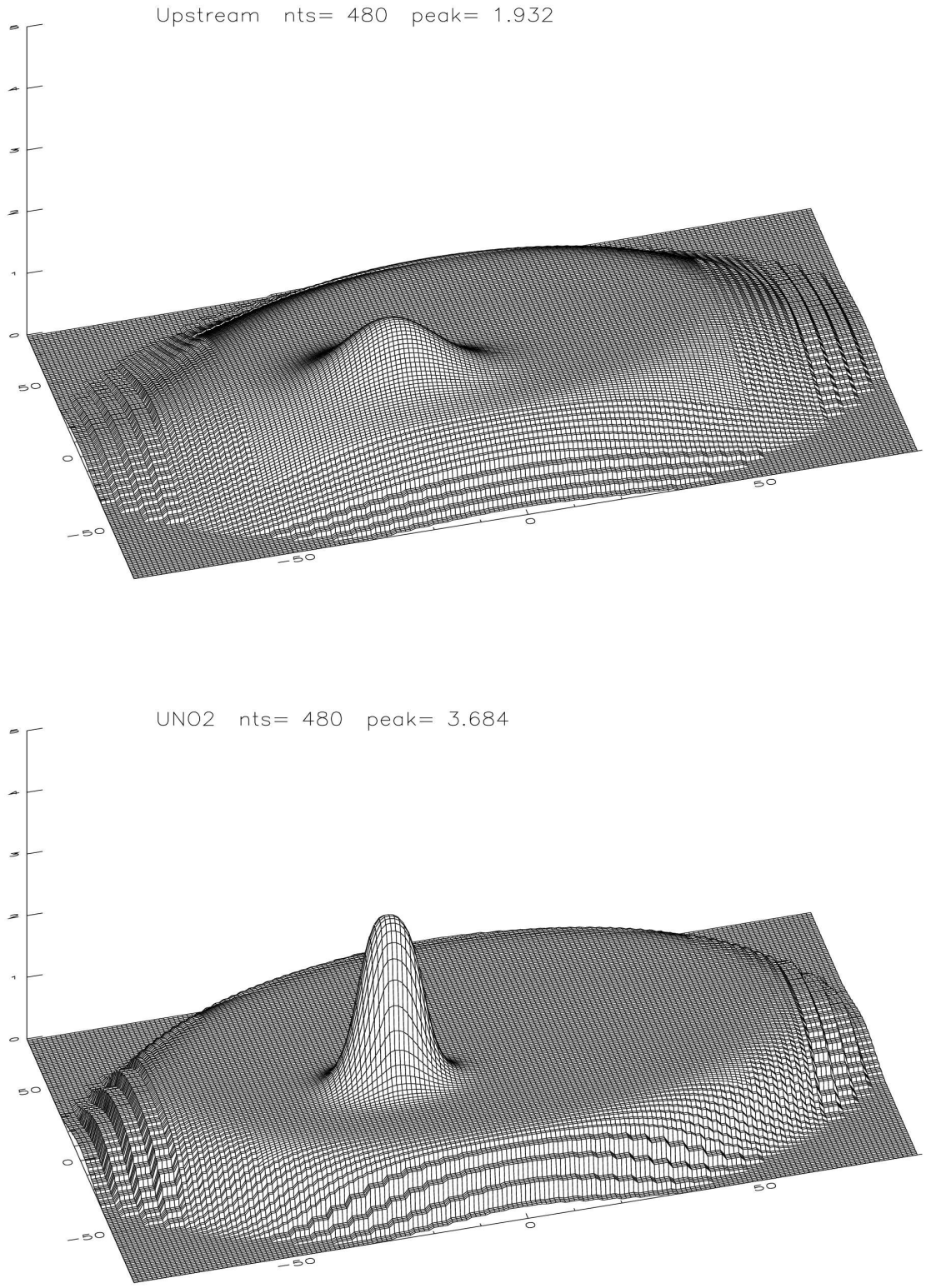

Fig.6. Solid roation test of the upstream and UNO2 schemes. Upper panel shows the upstream result and the lower panel UNO2 result after 1 rotation or 480 time steps. Initial condition is the same as shown in Fig. 5.

Fig. 7 illustrates the results by the UNO3 scheme in the two regimes. Panel (a) in Fig. 10 shows the initial cone used for the test (nts = 0). As the boundary condition does not affect the two central vertices spanned by the initial cone, only the central size 1 area is illustrated here. The cone has a base radius of 15 size 1 cells and height of 3.88 units and rests on a non-zero uniform background of 1 unit. Other panels in Fig. 7 show the subsequent time steps of 38, 76 and 380, corresponding to roughly 1/2, 1, and 5 times of *T*, respectively. The nts = 38 and 76 results may be considered to be in the first regime, which are comparable with the exact solution panel (b) and (d) in Fig. 3 of Staniforth et al. (1987). These results are also comparable to those of more complicated advection schemes, such as the MAPF scheme (Bott, 1993, Fig.1 (b) and (d)) and the high-order schemes (Leonard, 1996, Fig. 9 and 10).

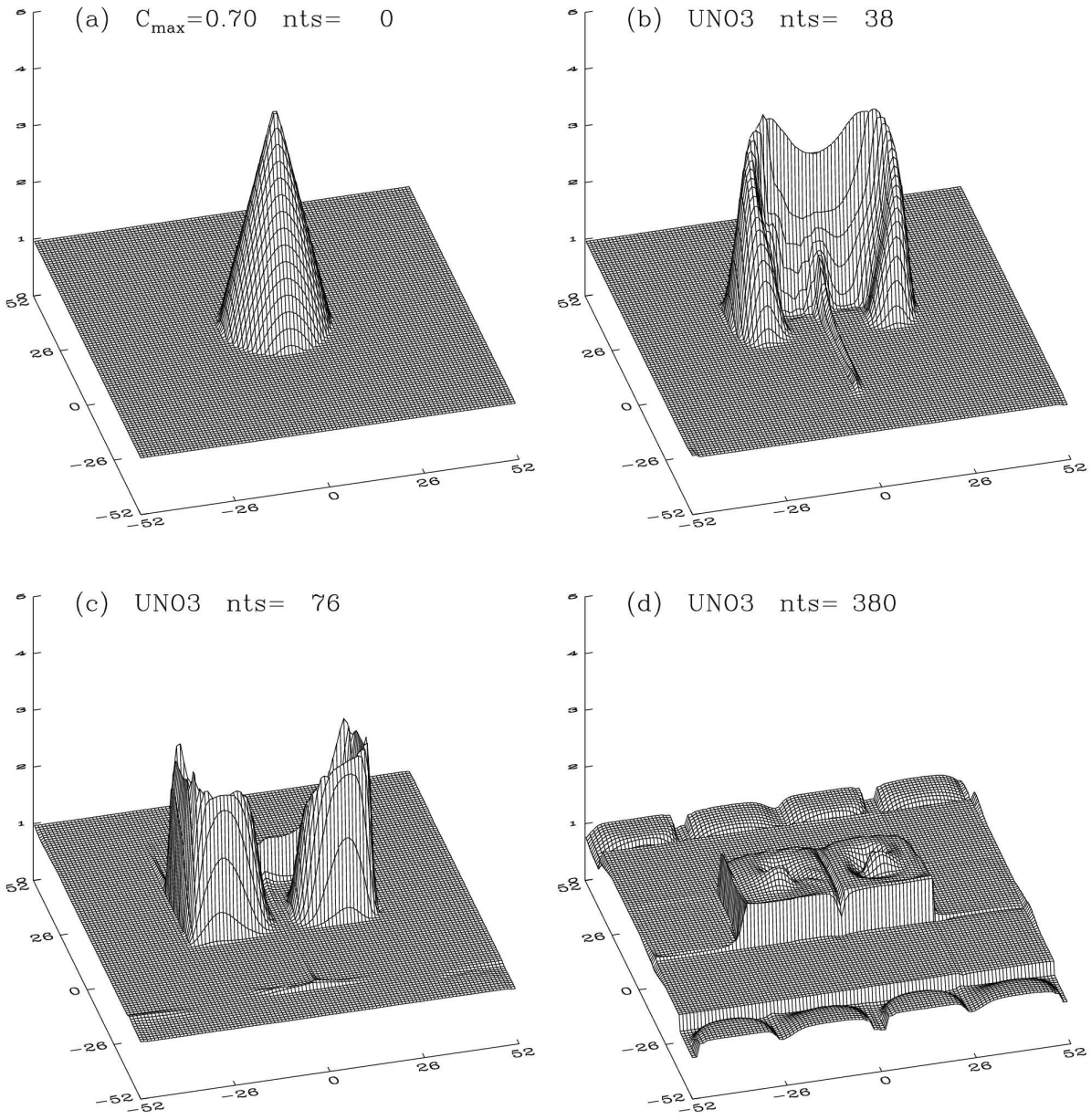

Fig. 7. Deformation test results by the UNO3 scheme. Panel (a) shows the initial cone and the uniform background in the central size-1 cell area of the multiple-cell grid. Other panels show the results after 38, 76 and 380 time steps, representing the two regimes of the deformation test.

Panel (d) in Fig. 7 for nts = 380 illustrates the numerical solution in the second regime, which shows the averaged features of the exact solution: two egg-cup shaped central vortices and strong gradient at the vortex boundaries. Other 10 vertices around the two central vertices are fully contained in the central size 1 area and maintained quite well the constancy of the uniform background. Outside vertices are subject to the boundary

condition and the initial uniform background was eroded by the boundary leak as shown by the four partial vertices in the lower and upper parts, respectively. The agreement of the UNO3 results with the exact solution is very satisfactory. The other three UNO schemes produce very similar deformation results (not shown here) except that the final egg-cup dips are shallower than the UNO3 ones due to increased numerical diffusion of these schemes.

5. Application in wave model

The UNO2 scheme has been substituted into the Met Office global wave model for comparison with the old advection scheme (Gadd 1978) and a 3rd order (ULT) scheme modified from the Takacs (1985) scheme with an upstream upper limiter (Li 2003). The ULT scheme has very similar performance as the UNO3 scheme in 1- and 2-D numerical tests. Comparison of wave model significant wave height (SWH) with Envisat altimeter (RA2) measurement indicated that the ULT result is in better agreement with satellite one than the Gadd scheme. But this comparison result is not shown here. This section concentrates on the comparison of the ULT and UNO2 scheme. Fig. 8 compares the Envisat SWH and wind speed along one satellite track on 19 May 2007 with the corresponding model results, using the two different advection schemes. The model results with ULT (red cross symbols) and UNO2 (green plus symbols) scheme are almost identical along the satellite track.

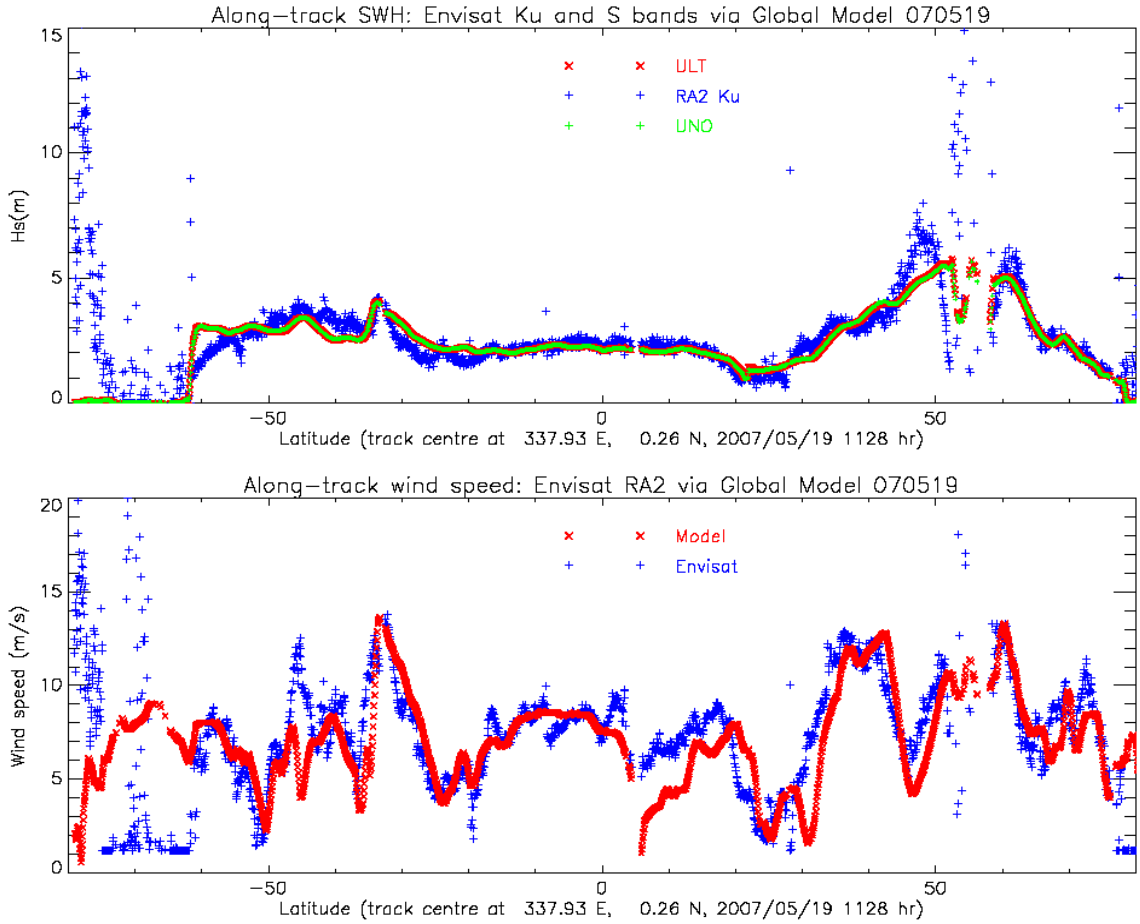

Fig. 8. Comparison of Envisat RA2 measurement with wave model using the UNO2 scheme and a 3rd order (ULT) scheme along one Envisat track on 19 May 2007. Upper panel shows the SWH and the lowerpanel is the wind speed.

Fig. 9 shows the scatter plots of the satellite SWH against the wave model in one month (May 2007) with the two advection schemes. The mean model SWH (2.809 m) with the ULT scheme (left panel in Fig. 9) is slightly lower thant that with the UNO2 scheme (2.811 m in the right panel). Nevertheless, both schemes result in the same rms error (0.705 m) against the satellite SWH. They also share the same correlation coefficient of 0.880. This nearly identical performace of the 2nd and 3rd order schemes in the global wave model may be attributed to the limited advection time steps for any given wave over an ocean basin scale. Taking a wave group speed of 10 m s^{-1}, for instance, it requires less than one week for the wave to travel cross the Atlantic basin (~

5000 km). If the advection time step is set as 5 min (as used in the Met Office global wave model), the total number of time steps over the one week period is about 2000, which is not long enough for the difference of the two schemes to manifest. So for the present model resolution (60 km), the UNO2 scheme is good enough for global surface wave transportation.

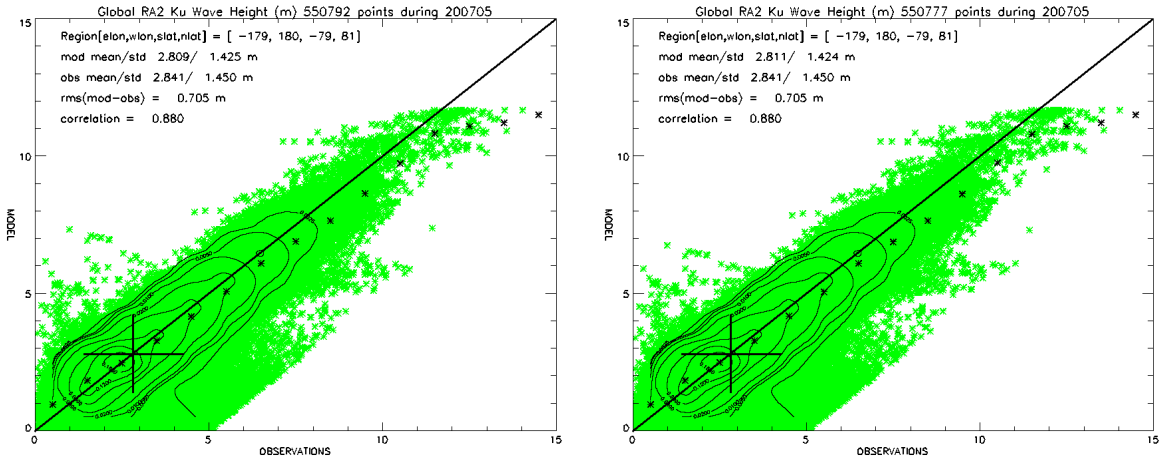

Fig. 9. Scatter plots of Envisat RA2 SWH against model values in May 2007. Wave model used the 3rd order ULT (left panel) and the UNO2 (right panel) advection schemes, respectively.

6. Summary and conclusions

Four simple upstream non-oscillatory advection schemes (UNO2, UNO2$^+$, UNO3$^-$, and UNO3) are derived by modifying existing classical advection schemes (the minmod (Roe 1985), the harmonic (van Leer 1977), the 3rd order scheme (Takacs 1985) and the ULTIMATE QUICKEST (Leonard 1991)). They are extended to 2-dimension flow by the MACHO approach (Leonard 1996) and to irregular grids in mid-flux interpolation form with symmetrical gradients. Uniform grid 1-D test is used to compare these UNO schemes with their classical counterparts and multiple-cell grid is used to test their irregular grid formulations. Classical 2-D rotation and deformation tests on multiple-cell grid are also applied on these schemes and results are satisfactory. The UNO schemes are consistent, conservative, shape-preserving and free from numerical oscillations. They also preserve constituent correlation of transported variables. The UNO2 is the simplest 2nd order non-oscillation scheme and may be used for advection and diffusion process when the real diffusion is large than the numerical diffusion of the UNO2 scheme, such as the tracer advection in the atmospheric boundary layer. Nevertheless, the numerical diffusion of the UNO2 scheme is much less than that of the 1st order upstream scheme. The UNO2 scheme is recommended for ocean surface wave model. The 3rd order UNO3 scheme has very small self-constrained diffusion and may be used for less diffusive advecetion process, like tracer transportation in the deep ocean.

Acknowledgments. The author is grateful to Dr Nigel Wood (Met Office, UK) for his constructive comments on this work.

REFERENCES

Allen, D.J., A.R. Douglass, R.B. Rood and P.D. Guthrie, 1991: Application of a monotonic upstream-biased transport scheme to three-dimensional constituent transport calculations. *Mon. Wea. Rev.*, **119**, 2456-2464.

Berger, M. and J. Oliger, 1984: Adaptive mesh refinement for hyperbolic partial differential equations. *J. Comput. Phys.*, **53**, 484-512.

Book, D.L., J. P. Boris and K. Hain, 1975: Flux corrected transport. II: Generalizations of the method. *J. Comput. Phys.*, **18**, 248-283.

Boris, J.P. and D.L. Book, 1973: Flux corrected transport I: SHASTA, a fluid transport algorithm that works. *J. Comput. Phys.*, **11**, 38-69.

Bott, A., 1992: Monotone flux limitation in the area-preserving flux-form advection algorithm. *Mon. Wea. Rev.*, **120**, 2592-2602.

Bott, A., 1993: The Monotone area-preserving flux-form advection algorithm: reducing the time-splitting error in two-dimensional fields. *Mon. Wea. Rev*., **121**, 2637-2641.

Colella, P., 1990: Multidimensional upwind methods for hyperbolic conservation laws. *J. Comput. Phys*., **87**, 171-200.

Colella, P. and P.R. Woodward, 1984: The piecewise parabolic method (PPM) for gas-dynamical simulations. *J. Comput. Phys*., **54**, 174-201.

Crowley, W.P., 1968: Numerical advection experiments. *Mon. Wea. Rev*., **96**, 1-11.

Davies, T., M.J.P. Cullen, A.J. Malcolm, M.H. Mawson, A. Staniforth, A.A. White and N. Wood, 2005: A new dynamical core for the Met Office's global and regional modelling of the atmosphere. *Q. J. R. Meteorol. Soc*., **131**, 1759-1782.

Fromm, J.E., 1968: A method for reducing dispersion in convective difference schemes. *J. Comput. Phys*., **3**, 176-189.

Gadd, A.J., 1978: A numerical advection scheme with small phase speed errors. *Q. J. R. Meteorol. Soc*., **104**, 583-594.

Godunov, S.K., 1959: Finite-difference methods for the numerical computations of equations of gas dynamics. *Math. Sb*., **47**, 271-290.

Harten, A. 1983: High resolution schemes for hyperbolic conservation laws. *J. Comput. Phys*. **49**, 357-393.

Harten, A., B. Engquist, S. Osher and S. Chakravarthy, 1987: Uniformly high order essentially non-oscillatory schemes, III, *J. Comput. Phys*. **71**, 231-303.

Holland, W.R., J.C. Chow and F.O. Bryan, 1998: Application of a third-order upwind scheme in the NCAR ocean model. *J. Climate*, **11**, 1487-1493.

Holm, E.V., 1995: A fully two-dimensional, non-oscillatory advection scheme for momentum and scalar transport equations. *Mon. Wea. Rev*., **123**, 536-552.

Hourdin, F. and A. Armengaud, 1999: The use of finite-volume methods for atmospheric advection of trace species. Part I: Test of various formulations in a general circulation model. *Mon. Wea. Rev*., **127**, 822-837.

Iselin, J.P., J. M. Prusa, W. J. Gutowski, 2002: Dynamic grid adaptation using the MPDATA scheme. *Mon. Wea. Rev*., **130**, 1026-1039.

Jiang, G.S. and C.W. Shu, 1996: Efficient implementation of weighted ENO schemes. *J. Comput. Phys*., **126**, 202-228.

Lax, P.D. and B. Wendroff, 1960: Systems of conservation laws. Comm. Pure Appl. Math, 13, 217-237.

Leonard, B. P., 1979: A stable and accurate conservative modelling procedure based on quadratic upstream interpolation. *Comput. Methods Appl. Mech. Eng*., **19**, 59-98.

Leonard, B.P., 1991: The ULTIMATE conservative difference scheme applied to unsteady one-dimensional advection. Computer Methods Appl. Mech. Eng., 88, 17-74.

Leonard, B.P., A.P. Lock and M.K. MacVean, 1996: Conservative explicit unrestricted-time-step multidimensional constancy-preserving advection schemes. *Mon. Wea. Rev*., **124**, 2588-2606.

Li, J.G. 2003: A multiple-cell flat-level model for atmospheric tracer dispersion over complex terrain. *Boundary-Layer Meteor*., **107**, 289-322.

Li, J.G., P.D. Killworth and D.A. Smeed, 2003: Response of an eddy-permitting ocean model to the assimilation of sparse in situ data. *J. Geophys. Res*., **108**, C4, 3111, 10pp.

Lin, S-J. and R.B. Rood, 1996: Multidimensional flux-form semi-Lagrangian transport schemes. *Mon. Wea. Rev*., **124**, 2046-2070.

Liu, X.-D., S. Osher and T. Chan, 1994: Weighted essentially non-oscillatory schemes. *J. Comput. Phys*., **115**, 200-212.

Prather, M.J., 1986: Numerical advection by conservation of second-order moments. *J. Geophys. Res*., **91**, 6671-6681.

Rasch, P.J., 1994: Conservative shape-preserving two-dimensional transport on a spherical reduced grid. *Mon. Wea. Rev*., **122**, 1337-1350.

Roe, P.L., 1981: Approximate Riemann solvers, parameter vectors and difference schemes. *J. Compu. Phys*., **43**, 357-372.

Roe, P.L., 1985: Large scale computations in fluid mechanics. *Lectures in Applied Mathematics* (E. Engquist, S. Osher and R.J.C. Sommerville Eds.), **22**, 163-193.

Smolarkiewicz, P.K., 1982: The multi-dimensional advection scheme. *Mon. Wea. Rev*., **110**, 1968-1983.

Smolarkiewicz, P.K., 1984: A fully multidimensional positive definite advection transport algorithm with small implicit diffusion. *J. Comput. Phys*., **54**, 325-362.

Smolarkiewicz, P.K. and W.W. Grabowski, 1990: The multidimensional positive definite advection transport algorithm: monoscillatory option. *J. Comput. Phys*., 86, 355-375.

Staniforth, A., J. Cote and J. Pudykiewicz, 1987: Comments on "Smolarkiewicz's deformation flow". *Mon. Wea. Rev.*, **115**, 894-900.

Sweby, P.K., 1984: High resolution schemes using flux limiters for hyperbolic conservation laws. *SIAM J. Numer. Anal.*, **21**, 995-1011.

Takacs, L.L., 1985: A two-step scheme for the advection equation with minimised dissipation and dispersion errors. *Mon. Wea. Rev.*, **113**, 1050-1065.

Thuburn, J., 1996: Multidimensional flux-limited advection schemes. *J. Comput. Phys.*, **123**, 74-83.

Thuburn, J., 1997: TVD schemes, positive schemes, and the universal limiter. *Mon. Wea. Rev.*, **125**, 1990-1993.

Tremback, C.J., J. Powell, W.R. Cotton and R.A. Pielke, 1987: The forward-in-time upstream advection scheme: extension to higher orders. *Mon. Wea. Rev.*, **115**, 540-555.

Tolman, H.L., B. Balasubramaniyan, L.D. Burroughs, D.V. Chalikov, Y.Y. Chao, H.S. Chen, and V.M. Gerald, 2002: Development and implementation of wind-generated ocean surface wave models at NCEP. *Weather and Forecasting*, **17**, 311-333.

Van Leer, B., 1974: Towards the ultimate conservative difference schemes. II: Monotonicity and conservation combined in a 2nd-order scheme. *J. Compu. Phys.*, **14**, 361-370.

Van Leer, B., 1977: Towards the ultimate conservative difference schemes. IV: A new approach to numerical convection. *J. Compu. Phys.*, **23**, 276-299.

Van Leer, B., 1979: Towards the ultimate conservative difference schemes. V: A second order sequel to Godanov's Method. *J. Compu. Phys.*, **32**, 101-136.

Walcek, C.J. and N.M. Aleksic, 1998: A simple but accurate mass conservative, peak-preserving, mixing ratio bounded advection algorithm with FORTRAN code. *Atmospheric Environment*, **32**, 3863-3880.

WAMDI group: S, Hasselmann, K. Hasselmann, E. Bauer, P.A.E.M. Janssen, G.J. Komen, L. Bertotti, P. Lionello, A. Guillaume, V.C. Cardone, J.A. Greenwood, M. Reistad, L. Zambresky and J.A. Ewing, 1988: The WAM model - a third generation ocean wave prediction model. *J. Phys. Oceanogr.*, **18**, 1775-1810.

Zalesak, S.T., 1979: Full multidimensional flux-corrected transport algorithms for fluids. *J. Comput. Phys.*, **31**, 335-362.